Reducing N2O induced cross-talk in a NDIR CO2 gas sensor for breath analysis using multilayer thin film optical interference coatings

Fleming, Lewis; Gibson, Des; Song, Shigeng; Li, Cheng; Reid, Stuart

Published in:
Surface & Coatings Technology

DOI:
10.1016/j.surfcoat.2017.09.033

Published: 25/02/2018

Document Version
Peer reviewed version

Manuscript cover page

Reducing N_2O induced cross-talk in a NDIR CO_2 gas sensor for breath analysis using multilayer thin film optical interference coatings

Lewis Fleming[a], Des Gibson[a,b], Shigeng Song[a], Cheng Li[a], Stuart Reid[a]

[a]Institute of Thin Films, Sensors and Imaging, School of Engineering and Computing, University of the West of Scotland, PA1 2BE Paisley, Scotland, UK

[b]Gas Sensing Solutions Ltd. 60 Grayshill Rd, Cumbernauld, Glasgow, G68 9HQ, Scotland UK

AUTHOR INFORMATION

Lewis.Fleming@uws.ac.uk

Des.Gibson@uws.ac.uk

Shigeng.Song@uws.ac.uk

Cheng.Li@uws.ac.uk

Stuart.Reid@uws.ac.uk

Corresponding Author

Lewis.Fleming@uws.ac.uk

Telephone number: +44(0)141 8494216

ABSTRACT

Carbon dioxide (CO_2) gas sensing is an important aspect in the biomedical field of capnography, where cheap, fast and accurate measurement of exhaled CO_2 vs. time is crucial in the evaluation of lung and tracheal function during surgical anaesthesia and is an under-used bio-marker for underlying respiratory conditions. Current detection methods do not adequately meet these requirements and suffer from considerable cross-talk associated with the commonly used anaesthetic gas nitrous oxide (N_2O). In this work, we report how cross-talk can be reduced in a commercially available, low power (35 mW) non-dispersive infrared (NDIR) CO_2 gas sensor using thin film multilayer optical filters. Current sensor spectral response, spans 2500 nm-5000 nm via use of a pentanary alloy LED/photodiode optopair grown by molecular beam epitaxy (MBE), resulting in sensor sensitivity to gases with absorption bands in this region, including N_2O. To reduce the effective spectral response of the sensor, capturing only CO_2, a multilayer thin film optical interference bandpass filter has been designed and deposited directly onto the diode epi-structures using microwave plasma assisted DC magnetron sputtering. Three different coating configurations have been explored; LED-only coated, photodiode only coated and both coated. Gas sensor response to N_2O for each coating configuration has been explored. It was found that application of an optical bandpass filter onto both the sensor LED and photodiode only was the most effective method of reducing sensor response to N_2O, however no signal was observed in one of the two "LED and PD coated", therefore optimal coating configuration for cross-talk reduction is subject to further investigation.

Keywords: CO_2 sensor, thin films, NDIR, mid-IR, microwave-assisted DC magnetron sputtering, multilayer optical interference filter, mid infrared light emitting diodes, mid infrared photodiodes, capnography, surgical anaesthesia, nitrous oxide, cross-talk, breath analysis

1. Introduction

In response to the increasing market need for a low cost, accurate, lightweight and portable CO_2 gas sensing modality measuring exhaled CO_2 as a function of time [1], a mid-IR photonics based CO_2 gas sensor has previously been described [2]. CO_2 gas sensing technology has been developed by Gas Sensing Solutions (GSS) ltd and has been employed in indoor air quality monitoring (IAQ), energy conservation in buildings, transport systems, industrial safety, medical capnography and horticulture [3]. Calls by the national institute for health and clinical excellence (NICE) have been made to increase exhaled CO_2 monitoring wherever possible [4–8] as respiratory rate and shape of a patients exhaled CO_2 versus time waveform can be key indicators of patient status to healthcare professionals and can allow for early stage medical intervention and reduction of future healthcare costs. Infrared breath CO_2 monitoring is currently being introduced for clinical use and has proved to be consistent with time tested gas sensing modalities such as mass spectrometry [9–11]. An IR CO_2 sensor as described by Gibson *et al* [3] may be a suitable candidate for exhaled CO_2 monitoring during surgical anaesthesia [12], due to its many advantages over current CO_2 monitoring techniques such as mass spectrometry. These advantages include rapid breath-by-breath analysis as a result of the 20 Hz measurement speed, in addition longevity (>15 years) and 35 mW operating power. The rapid 20 Hz measurement speed enabled by rapid modulation of the sensor LED, has allowed for new diagnostic applications in the medical and veterinary arena. A crucial limitation of the CO_2 gas sensing technique described in this work with respect to use in surgical anaesthesia is the spectral sensitivity. The spectral sensitivity ranges from 2500 nm to 5000 nm without optical filtering, which is narrower as compared with standard high power thermal source NDIR gas sensors, however still broad enough to capture the

absorption bands of a few gases which exhibit molecular vibrational absorptions in this region, including water (H_2O) methane (CH_4) and nitrous oxide (N_2O).

As a result, the gas sensor is sensitive to N_2O and in its current configuration is unsuitable for accurate CO_2 monitoring for surgery patients undergoing general anesthesia. Figure 1 (a) shows a schematic of the gas sensor in its current configuration. Utilizing an LED–photodiode optopair is advantageous as compared with standard thermal source NDIR gas sensing methods due to the low power consumption (35 mW [13] for GSS Ltd CO_2 sensor technology as compared with typically 100 – 560 mW for thermal source/pyroelectric or thermopile detectors [3,14,15]). The gas sensor has 3 main components; 2 epitaxially grown hetereostructure diodes mounted side by side, less than 1 mm apart integrated onto a small 1 mm x 2 mm bridgeboard. The bridgeboard is mounted, diode side up, facing an injection molded gold coated plastic optical dome. The diodes, in forward and reverse bias respectively, behave as one light-emitting diode (LED) and one photodiode and are based on a pentanary alloy AlGaInAsSb narrow bandgap III-V material combination grown by molecular beam epitaxy (MBE) [1,16,17]. Mid-IR radiation is emitted from the LED is reflected off the gold coated optical dome and then incident on the photodiode resulting in a photodiode photocurrent response. The photodiode photocurrent response is maximal when no absorbing gas is present inside the dome. When a mid-IR absorbing gas is present, such as CO_2, radiation emitted from the LED is absorbed in proportion to the concentration of gas in the dome resulting in a reduction in signal proportional to the gas concentration.

Spectral emission and detection ranges of the LED and photodiode respectively can be tuned by altering alloy composition, and have been tuned to emit and detect over the 4260 nm region at which the CO_2 molecule exhibits its O=C=O asymmetric stretch absorption band. Neighbouring the 4260 nm CO_2 absorption band is a fundamental N_2O absorption band

centred around 4500 nm [18] which lies within the sensor's 2500 nm to 5000 nm spectral detection range and is responsible for unwanted crosstalk in the sensor when N_2O is present inside the gas sensor. The sensor spectral response, CO_2 and N_2O absorption bands are shown in figure 2. It can be seen that the spectral response overlaps both the CO_2 and N_2O absorption bands. By optically filtering the emission from the LED, in order to reduce the bandwidth of the light incident on the photodiode, the senor will become less sensitive to N_2O as no N_2O absorbing wavelengths are present to induce a photocurrent in the photodiode. By incorporating such optical filtering into the gas sensor architecture, sensor sensitivity to CO2 can be made to be dominant with respect to other gases present during surgical anaesthesia where cross-talk inducing anaesthetic N_2O gas may be present as a result of patient exhalation of N_2O that has been delivered to induce general anaesthesia. The aim of this work is to realise an optical filter to be incorporated directly into the gas sensor architecture using a technique that can easily be incorporated aligns with high throughput gas sensor production. In the next section, a pulsed-DC sputtering system assisted with microwave plasma (3 kW power) used in this work to grow thin film optical interference filters at room temperature directly onto the diode heterostructures is described.

2. Materials and methods

2.1 Single and multilayer thin film preparation method

Thin film optical coatings were grown using microwave plasma assisted DC magnetron sputtering. The system used to deposit optical interference filters in this work has previously been described by Song and Li *et al* and the successful deposition of various commonly encountered optical materials for both visible are IR wavelengths has been demonstrated [19–22]. The system utilizes a drum based system where substrates to be deposited on are mounted onto a rotating drum. The substrates sweep past two targets situated at opposite ends of the chamber and past a 3 kW microwave source located at the top of the chamber used in order to split molecular oxygen into atomic oxygen, resulting in improved oxidation of oxide films and lower optical absorption. Power is supplied to each target using two advanced energy pulsed DC MDX-20 kW magnetron drive power supplies. Gas flow is controlled using an MKS multigas controller. The system exhibits a base pressure of approximately ~$5\times^{-7}$ Torr. For this work, germanium (Ge) and niobium (Nb) targets were sputtered from in order to deposit layers of thin film Ge and Nb_2O_5. The system is fitted with a Meissner trap, cooled using a Telemark cryogenics 3600 polycold cryo-cooler unit used to freeze and trap residual water vapour in the vacuum chamber, which is difficult to eliminate using turbomolecular pumping alone. Heated water is passed through the chamber walls resulting in further evaporation of attached water vapour and organic contamination increasing the likelihood of trapping on the cryo-cooled coils. Using this system, single layer thin film materials (Ge and Nb_2O_5) were deposited onto <111> p-type silicon (Si) wafer substrates for optical characterisation and also onto zinc selenide (ZnSe) for destructive testing. Then, multilayer thin film optical coatings were deposited onto gas sensor bridgeboards hosting the sensor's LED and photodiode.

2.2 Thin film design and optical characterisation

Multilayer bandpass filters were designed and optimised using the Essential Macleod thin film design software. Three different coating configurations were explored; LED-only coated (photodiode masked), photodiode-only coated (LED masked) and both coated (no masking). The electroluminescence (EL) of the LEDs, and the photocurrent response of the photodiodes, prior to and after coating were measured using a Bruker VERTEX 70/70v Fourier Transform Infrared (FTIR) spectrometer. For each coating run, <111> silicon (Si) wafer substrates were loaded into the chamber as witness samples and measured after coating using a Nicolet iS-50 Fourier Transform Infrared (FTIR) spectrometer.

2.3 SEM & EDX analysis

Cross-sectional images of the deposited single and multilayer thin films were obtained using scanning electron microscopy (SEM). Analysis was performed on a Hitatchi S-4100 scanning electron microscope at an acceleration voltage of 10 kV. Single layer film composition was confirmed by energy dispersive X-ray (EDX) analysis on an Oxford Instruments X-Max 80 detector at an acceleration voltage of 30 kV.

2.4 Coated gas sensor testing

Coated sensor bridgeboards were then built into SprintIR 20 Hz CO_2 Sensors by Gas Sensing Solutions Ltd. In order to test the coated sensor response to N_2O, gas mixtures of N_2/N_2O were fed into a sealed aluminium chamber containing the sensor to be tested, using an MKS Instruments 647B controller which was used to control two MKS MFCs, one for N_2 and one for N_2O. Sensor response to N_2O was recorded using Gas Sensing Solutions' firmware. A schematic of the gas sensor testbed is shown in figure 4.

3. Results and discussion

3.1 Single layer deposition and optical characterisation

In order to model a multilayer optical interference bandpass filter, the optical constants of the constituent individual layers were extracted. Using the deposition conditions displayed in Table 1, single layers of Ge and Nb_2O_5 were each sputter deposited onto <111> silicon (Si) wafer substrates. The mid-IR optical transmittance spectrum for each of these samples was measured over a wavelength range of 2500 nm to 25000 nm using FTIR. The transmittance spectra are shown in figure 4 for Ge on Si and Nb_2O_5 on Si. The bare Si wafer substrate transmittance is also plotted. Figure 6 shows the optical constants used in the multilayer design for these materials. The optical constants shown figure 6 were used to model a multilayer thin film optical interference bandpass filter, with a passband centred at 4260 nm. Cross-sectional imaging of these samples was obtained using SEM and are shown in Figure 7 for a 15,000 times magnification. In addition to the refractive index values obtained for these samples, which serves an indicator that these coatings are indeed pure (high quality) Ge and Nb_2O_5, EDX analysis was performed on the samples to further confirm the successful deposition of these materials in thin film form. EDX for both samples is shown in Figure 8. For the Ge sample, peaks were observed for Ge, zinc (Zn) and selenium (Se) – confirming the presence of Ge. The Zn and Se peaks are highly likely to be attributable to the ZnSe substrate on which the coating was deposited. For the Nb_2O_5 sample, the presence of niobium (Nb) and oxygen (O) was confirmed. Peaks were also observed for argon (Ar), tantalum (Ta), Zn and Se. The presence of small amounts of argon is suspected to be due to argon ion implantation in the film as a result of Ar being used as the process sputtering gas. Again, Zn and Se signals are suspected to be from the substrate. Incorporation of a small amount of Ta is likely to be due to accidental sputtering of Ta present on the target masking as this system has previously been used to deposit Ta containing thin films. Given the small height of the peak, the

concentration of Ta in the film appears to be minimal, and appears to have little effect on the refractive index which, in any case, is the important optical parameter and was found to be close to bulk Nb_2O_5. A Ge/Nb_2O_5 material combination was chosen as these coating materials exhibit a high degree of optical transparency in the mid-IR region of interest. One advantage of choosing Ge/Nb_2O_5 is that bandpass filters fabricated from this material combination exhibit a comparatively low spectral shift for angles of incidence away from normal, which is important for this application, as the LED used in this sensor has a planar geometry with a lambertian emission pattern which has sizeable emission intensity out to higher angles (maintaining around 50% of normal intensity at an angle of 60^{O}). This means that the light emitted/detected at higher angles will still be passed by the passband of filter, allowing for improved SNR.

3.2 Multilayer optical interference filter design

A 3-cavity Fabry-Perot starting design was chosen and then optimised in order to broaden the bandwidth and maximise the optical transmittance to capture the entire CO_2 absorption band. This yielded a 22-layer multilayer filter design with a transmittance spectrum shown in Figure 9 with a centre wavelength (CWL) of 4260 nm and a peak transmittance of 60%. This model is for a coating on substrate where back-face reflection losses are present. As the coatings are applied directly onto the LED or photodiode structures directly, no back-face reflection losses occur, therefore an increase of around 30% can be expected boosting the optical transmittance to around 90%. Reflection of light occurs at interfaces where a refractive index contrast is present on either side. Back-face reflection losses occur for a film-on-substrate assembly with air as the exit medium; a sizable reflection of light occurs at the substrate-air interface as a result of the high refractive index contrast between the substrate and exit medium. This reflection reduces the total amount of light transmitted through the sample.

By applying the coating directly onto the photodiode, the light passing the film-substrate interface is absorbed by the active region of the photodiode (which behaves as the substrate) instead of being reflected by an extra substrate-exit medium interface which would be present for a film-on-substrate in air assembly. Therefore, applying the coating directly onto the photodiode reduces the number of interfaces the light must cross and therefore the number of reflections (in which transmitted light is lost) before the light is incident on the active region of the photodiode. Therefore, applying the coating directly onto the photodiode increases the intensity of transmitted IR light as compared with having a separate film-on-substrate filter fixed separately somewhere in between the LED and photodiode. The reverse case is also true; one less interface reflection is present for the coating on the LED as compared with having a separate film on substrate assembly in front of the LED.

In addition to bandpass filters for the reduction of cross-talk in a CO_2 gas sensor, work has also been carried out for producing bandpass filters in the interest of methane gas detection for sensors utilizing the same technology as the aforementioned CO_2 gas sensor with the only difference being that the LED EL and photodiode photocurrent responses were tuned for peak spectral response at 3300 nm corresponding to a principle absorption band of CH_4, which is also plotted in Figure 9. These optical coatings were applied to sensor LEDs and photodiodes for CO_2 gas and CH_4 sensors respectively. The CO_2 LEDs and photodiodes were coated with sample H17C17124 and the CH_4 LEDs and photodiodes were coated with sample H17C131805. Cross-sectional SEM images were obtained for each multilayer optical filter structure and are shown in Figure 7.

3.3 LED EL and photodiode photocurrent response before and after coating

Figures 10 shows CO_2 sensor LED EL and photodiode photocurrent response before and after application of the multilayer optical coating, sample H17C17124. It can be seen, from Figures 7 and 8 that the bandwidth of the LED EL and the photodiode photocurrent response has been reduced in accordance with the shape of the optical interference filter spectral characteristic of sample H17C17124. The absorption feature observed at 4260 nm is an artefact of atmospheric CO_2 in the FTIR measurement system. For both the LED and the photodiode, the magnitude of the response at 4500 nm has successfully been reduced in order to minimise sensor sensitivity to N_2O. Figure 11 shows the coated and uncoated LED and photodiodes for the CH_4 sensor respectively. A similar case is seen for the CH_4 LEDs and photodiodes where the LED EL and photodiode photocurrent response bandwidth has been reduced in accordance with the spectral characteristic of the deposited H17C131805 optical interference spectrum.

3.4 Coated gas sensor response to nitrous oxide

The three different coating configurations were applied to two bridgeboards each and built into gas sensors yielding 6 sensors to be tested. The coated CO_2 gas sensors were tested in the gas sensor testbed for a 0% -100% N_2O gas concentration range and also for a 0% -20% CO_2 gas concentration range. For each gas sensor 300 measurements were taken at each CO2 and N2O gas concentration and the root-mean-square (RMS) signal was calculated. The standard deviation (RMS noise) was also calculated from this data. The RMS signal for N2O and RMS noise data for CO2 are shown in figures 13 and 14 respectively. Sensor 1 is not shown as no signal was measured from this sensor. The N2O signal response is lowest for sensor 2 followed by sensors 6, 5, 3, 4 and lastly the uncoated. It is believed that sensor 2 has the lowest response because this sensor had both the LED and photodiode coated, resulting in twice the amount of blocking at the N2O associated wavelength as compared with the singly coated sensors. Sensor 2, however, exhibits much greater noise than the others on account of a

low IR intensity on the photodiode and therefore a lower SNR. The photodiode-only coated sensors (5 and 6) are less sensitive to N2O as compared with the LED-only coated (3 and 4). This can be accounted for by the fact that the coated LED EL has a slightly broader bandwidth than the coated photodiode photocurrent response, resulting in a higher intensity at the small 3900 nm N2O associated wavelength (as can be seen from figure 2). The exact reason for this broader bandwidth is unclear, however the author suggests the following reason; the coated photodiode is more true to the normal incidence shape of the optical filter transmittance spectral characteristic because the light is focussed closer to normal incidence. Emission from the LED is highly angular - the LED has a lambertian emission pattern so the the coated LED spectral characteristic will include a greater contribution from the optical filter spectral characteristic at higher angles (a slight blue-shift), which accounts for the slower fall off on the left hand side (cut-on) portion of the LED EL curve. This accounts for the slightly "fatter" LED EL curve as compared with the coated photodiode photocurrent response curve. The higher intensity on the left hand fall off results in a higher intensity at the small 3900 nm N2O associated band, resulting in an increased sensitivity to N2O. The broader LED EL also accounts for the lower noise for LED-only coated sensors (3 and 4) as compared with sensors 5 and 6 (photodiode-only coated) as a greater intensity of IR light is incident on the photodiode active region for LED-only coated. We suggest that application of the optical coating onto the photodiode only may be the best approach for N2O cross-talk reduction on account of the better blocking of N2O associated wavelengths as compared with the LED-only coated sensor and also the lower noise as compared with the both-coated sensor.

4. Conclusion

In this work, multilayer thin film optical interference bandpass filters were deposited onto epitaxially grown heterostructure mid-IR LEDs and photodiodes using microwave-plasma assisted pulsed DC magnetron sputtering. By application of the optical bandpass filters, it is demonstrated that the emission and detection bandwidths of the diode spectral responses (LED EL and photodiode photocurrent response) were successfully reduced, eliminating CO_2 gas sensor cross-talk response to N_2O. Coatings were also applied to diodes grown in the interest of CH_4 gas detection with similar results achieved. Coated CO_2 gas sensor bridgeboards each hosting an LED and photodiode were built into currently existing GSS Ltd. CO_2 gas sensors and three different optical coating configurations explored; 1) LED only coated, 2) photodiode only coated and 3) both LED and photodiode coated. Each configuration was applied to two LED/photodiode bridgeboards. Coated sensors had their response to N_2O tested in a gas sensor test-bed and it was shown that cross-talk was successfully reduced in all coated sensors. Sensor 2 had the lowest response to N_2O followed by 5, 6, 3, 4 then uncoated. Sensor 2 displayed the highest noise under CO_2 measurement, followed by sensors 5 and 6 then 3 and 4 with the uncoated having the lowest noise.

A next stage to this work will involve testing the coated gas sensors in a novel CO_2 breath emulation system [2] mimicking human exhaled CO_2 versus time waveforms is planned and will be published in a future work. The breath emulation system has a port for the introduction of anaesthetic N_2O, mimicking the human exhalation conditions observed when

anaesthetic N_2O is introduced to a patient under general anaesthesia. The breath emulation apparatus has previously been used to test CO_2 gas sensor performance as part of a patented hand-held capnometer device for point-of-care diagnostics [23].

Acknowledgements

We would like to thank The Royal Society (RS), the Society of Chemical Industry (SCI) and Gas Sensing Solutions (GSS) Ltd. for the Industrial PhD studentship and financial support. The author would also like to extend gratitude towards the Society of Vacuum Coaters (SVC) for the sponsored student award, which provided the opportunity to present this work at the 60^{th} Annual SVC TechCon 2017 in Providence, Rhode Island.

References

[1] M. Folke, L. Cernerud, M. Ekström, B. Hök, Critical review of non-invasive respiratory monitoring in medical care, Med. Biol. Eng. Comput. 41 (2003) 377–83. doi:10.1007/BF02348078.

[2] L. Fleming, D. Gibson, S. Song, D. Hutson, S. Reid, C. MacGregor, C. Clark, One-dimensional photonic crystals for eliminating cross-talk in mid-IR photonics-based respiratory gas sensing, Proc. SPIE 10103, Terahertz, RF, Millimeter, Submillimeter-Wave Technol. Appl. X. 10103 (2017) 1010318. doi:10.1117/12.2247851.

[3] D. Gibson, C. MacGregor, A novel solid state non-dispersive infrared CO2 gas sensor compatible with wireless and portable deployment, Sensors. 13 (2013) 7079–7103. doi:10.3390/s130607079.

[4] M.A. Cretikos, R. Bellomo, K. Hillman, J. Chen, S. Finfer, A. Flabouris, Respiratory rate: The neglected vital sign, Med. J. Aust. 188 (2008) 657–659. doi:cre11027_fm [pii].

[5] M. Cretikos, J. Chen, K. Hillman, R. Bellomo, S. Finfer, A. Flabouris, The objective medical emergency team activation criteria: A case-control study, Resuscitation. 73 (2007) 62–72. doi:10.1016/j.resuscitation.2006.08.020.

[6] R. Parkes, Rate of respiration: The forgotten vital sign, Emerg. Nurse. 19 (2011) 12–17. doi:10.7748/en2011.05.19.2.12.c8504.

[7] P. Barthel, R. Wensel, A. Bauer, A. Müller, P. Wolf, K. Ulm, K.M. Huster, D.P. Francis, M. Malik, G. Schmidt, Respiratory rate predicts outcome after acute myocardial infarction: A prospective cohort study, Eur. Heart J. 34 (2013) 1644–1650. doi:10.1093/eurheartj/ehs420.

[8] D.R. Goldhill, A.F. McNarry, Physiological abnormalities in early warning scores are related to mortality in adult inpatients, Br. J. Anaesth. 92 (2004) 882–884. doi:10.1093/bja/aeh113.

[9] N.. Luff, D.. White, Evaluation of the Datex “Normac” anaesthetic agent monitor, Anaesthesia. 40 (1985) 555–559.

[10] H. Mcpeak, E. Palayiwa, R. Madgwick, M. Skyes, Evaluation of a multigas anaesthetic monitor: The Datex Capnomac, Anaesthesia. 43 (1989) 1035–1041. doi:10.1111/j.1365-2044.1988.tb05705.x.

[11] M.B. Jaffe, Mainstream or Sidestream Capnography ?, Respironics. (2002) 1–14. http://www.oem.respironics.com/Downloads/Main vs Side.pdf.

[12] K. Bhavani-shankar, H. Moseley, A. Kumar, Y. Delph, Review Article Capnometry and anaesthesia, Can. J. Anaesth. 36 (1992) 617–632. doi:10.1007/BF03008330.

[13] Gas Sensing Solutions Ltd, GSS SprintIR High Speed Carbon Dioxide Sensor datasheet, 2016.

[14] ELT sensor corp, ELT Sensor, (2014). http://eltsensor.co.kr/2012/kor/pdf/S-100/DS_S-100_Rev 2.8.pdf.

[15] Optosense, Optosense AS, (n.d.). http://static1.1.sqspcdn.com/static/f/193715/15932596/1326061207233/OptoSense+-+English+flyer.pdf?token=7pVfzFjaadVrNeqGkA7RrdIIiB0%3D.

[16] M.K. Haigh, G.R. Nash, T. Terakado, N. Bando, Y. Yamagishi, S.J. Smith, L. Buckle, M.T. Emeny, T. Ashley, Mid-infrared AlxIn1-xSb components for gas sensing, J. Phys. Conf. Ser. 76 (2007) 1–5. doi:10.1088/1742-6596/76/1/012003.

[17] M. Kesaria, M. de la Mare, A. Krier, Room temperature mid-infrared InAsSbN multi-quantum well photodiodes grown by MBE, J. Phys. D. Appl. Phys. 49 (2016) 6. doi:10.1088/0022-3727/49/43/435107.

[18] L.S. Rothman et al, The HITRAN 2008 molecular spectroscopic database, J. Quant. Spectrosc. Radiat. Transf. 110 (2009) 533–572. doi:10.1016/j.jqsrt.2009.02.013.

[19] C. Li, S. Song, D. Gibson, D. Child, H. Chu, Waddel E, Modeling and validation of uniform large-area optical coating deposition on a rotating drum using microwave plasma reactive sputtering, Appl. Opt. 56 (2017) 65–70. doi:https://doi.org/10.1364/AO.56.000C65.

[20] S. Song, C. Li, H. Chu, D. Gibson, Reactive dynamics analysis of critical Nb2O5 sputtering rate for drum-based metal-like deposition, Appl. Opt. 56 (2017) 206–210. doi:https://doi.org/10.1364/AO.56.00C206.

[21] Y. Alajlani, F. Placido, D. Gibson, H.O. Chu, S. Song, L. Porteous, S. Moh, Nanostructured ZnO films prepared by hydro-thermal chemical deposition and microwave-activated reactive

sputtering, Surf. Coatings Technol. 290 (2016) 16–20. doi:10.1016/j.surfcoat.2016.01.036.
[22] D. Gibson, S. Song, C. Li, D. Child, Optical properties of sputter deposited amorphous hydrogenated silicon films, Opt. Interf. Coatings OSA Tech. Dig. (2016). doi:https://doi.org/10.1364/OIC.2016.ThC.2.
[23] N. Patel, J. Carter, J. Walsh, R. Overend, C. Mcgregor, D. Gibson, E. Wadell, Fast response capnometer for diagnosis and management of respiratory conditions UK1421961.2, WO/2016/092308, 2016.

Table I. Deposition process parameters for the growth of Ge and Nb_2O_5 thin films. These parameters yielded the smooth, spectrally stable optical interference fringes shown in figure 4.

Condition	**Ge**	**Nb_2O_5**
Ar flow rate ($sccm^{-1}$)	189	189
O_2 flow rate ($sccm^{-1}$)	0	78
Ar partial pressure (mTorr)	4.52	4.52
O_2 partial pressure	0	0.9
MDX Power (kW)	2.6	2.9
MDX Current (A)	4	9.5
MDX Voltage (V)	650	307

Table II. Signal values for different coating configurations at 36.36% N_2O gas concentration. Sensor 2 has the lowest value followed by 6 then 5. Sensor 2 has a reduced SNR performance due to being doubly coated. Sensor 1 yielded no signal. For these reasons we suggest that coating the photodiode-only may be the most effective and risk-free method of N_2O cross-talk reduction.

Sensor #	**Signal at 36.36% N_2O concentration (a.u.)**
Uncoated	1908.27
2 (both-coated)	81.97
3 (LED-only)	303.73
4 (LED-only)	353.38
5 (photodiode-only)	192.85
6 (photodiode-only)	116.83

Figure 1. Coated gas sensor schematics

CO_2 gas sensor architecture for (a) the gas sensor in its current configuration, with no applied optical coating over the diodes and (b) the new modified gas sensor architecture by application of optical coating to the bridgeboard using microwave-assisted DC magnetron sputtering.

Figure 2. Sensor spectral response and gas absorption coefficients

Total sensor spectral response and CO_2 and N_2O absorption coefficients. It can be seen that the total response spans 2500 nm – 5000 nm with peak sensitivity coinciding with the CWL of the 4260 nm CO_2 absorption band. N_2O exhibits a strong absorption centred at 4500 nm also lying within the spectral response, resulting in sensor sensitivity to N_2O also.

Figure 3. Thin film deposition system

Schematic of the microwave-assisted DC magnetron sputtering system used in this work, the Microdyn. A sputtered flux is incident onto substrates mounted onto the rotating drum (60 RPM) during deposition. A microwave source is used to facilitate a greater plasma density for the reactive gas species resulting in improved oxygen plasma reactivity and uniform oxidation of the growing film.

Figure 4. Gas sensor testing apparatus

Gas flow circuit schematic used in the gas sensor testbed. N_2O concentration in the aluminium chamber was controlled by flowing varying ratios of N_2 and N_2O. N_2 is IR inactive and does not elicit a response from the sensor.

Figure 5. Single layer transmittance spectra

Optical transmittance spectra for single layer Ge and single layer Nb_2O_5, both on 0.5 mm thick <111> Si wafer substrates. The observed interference fringes indicate the deposition of single layers and were fit to obtain the material optical constants of the film.

Figure 6. Material optical constants

Optical constants (refractive index (n) and extinction coefficient (κ)) obtained for single thin film layers of (a) Ge and (b) Nb_2O_5 deposited using the deposition parameters displayed in table 1. Values obtained are similar to those found in the literature. The optical constants were used in the modelling of the multilayer interference filter.

Figure 7. Single layer SEM

Cross-sectional SEM images of single layer (a) single layer Ge and (b) single layer Nb_2O_5 taken at 15,000 X magnification.

Figure 8. Elemental analysis

EDX spectra confirming the presence of Ge and Nb_2O_5 for (a) single layer Ge on ZnSe witness piece and (b) single layer Nb_2O_5 on ZnSe witness piece. Peaks for Zn and Se are attributed to the substrate. Argon was detected as it is suspected that a small amount of the process gas may be incorporated into the film. Some Ta appears to be present in the film and it is proposed that this is re-sputtered material from tooling in the deposition chamber. A 30 keV beam energy was used.

Figure 9. Multilayer optical filter transmittance

Optical transmittance versus wavelength spectra for witness silicon substrate samples present for the H17C131805 and H17C171240 CH_4 and CO_2 filter coating runs. Both samples exhibit a bandpass filter centred at 3300 nm and 4260 nm in order to capture the absorption bands of CH_4 and CO_2 respectively. The CO_2 and CH_4 absorption bands are shown for comparison.

Figure 10. Multilayer SEM

Cross-sectional SEM images for (a) CO_2 filter, witness sample H17C171240 and (b) CH_4 filter, witness sample H17C131805

Figure 11. CO_2 sensor LED and photodiode coatings

(a) CO_2 LED EL and (b) photodiode photocurrent response before and after application of the multilayer optical coating, sample H17C171240. It appears that by application of the coating, the bandwidths of these spectral repsonses have been reduced and approach the shape of the transmittance spectrum of the optical filter witness sample. In both cases, the magnitude of spectral response was reduced at 4500 nm.

Figure 12. CH_4 sensor LED and photodiode coatings

(a) CH_4 sensor LED EL and (b) photodiode photocurrent response before and after application of the multilayer optical coating, sample H17C131805. Similarly with the CO_2 LED and photodiode, the bandwidth of the spectral responses have been reduced in accordance with the applied optical filter spectral characteristic in order to reduce sensor sensitivity to other gases with absorption bands in this spectral region.

Figure 13. Coated gas sensor response to N_2O & noise response to CO_2

(a) CO_2 gas sensor RMS signal response to N_2O and (b) calculated noise for CO_2 for the three different bridgeboard coating configurations. From this, it appears that application of the coating to both the LED and photodiode has the greatest N_2O induced cross-talk reduction effect coupled with the largest noise.

Figure 14. Overlay of coated LED EL, photodiode photocurrent response and optical filter transmittance spectrum

Comparison of the different diode spectral responses, highlighting the curve shape conformity to the optical filter spectral characteristic. The slight difference between the LED EL and photodiode photocurrent response is clear from this plot.

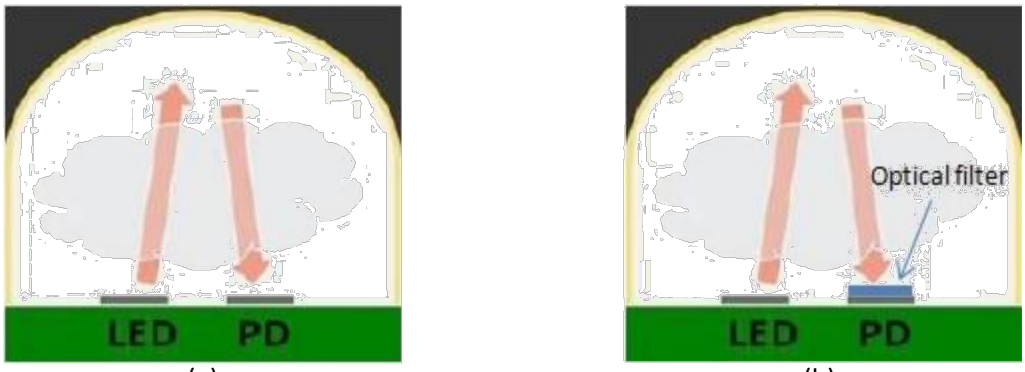
LED
PD
Optical filter
LED
PD

(a) (b)

1.

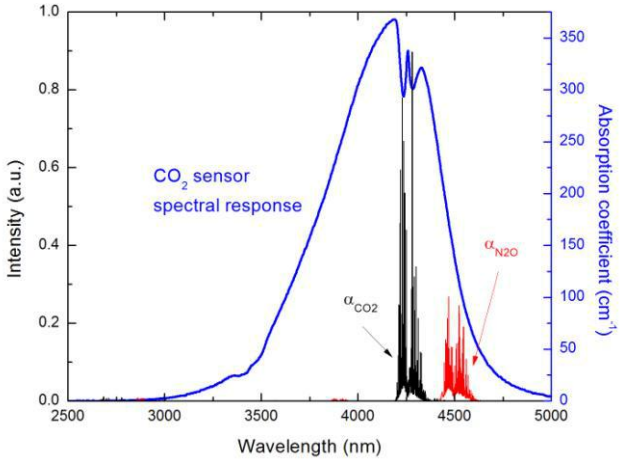
CO2 sensor
spectral response
αCO2
αN2O
Intensity (a.u.)
Absorption coefficient (cm-1)
Wavelength (nm)
1.0
0.8
0.6
0.4
0.2
0.0
350
300
250
200
150
100
50
0
2500
3000
3500
4000
4500
5000

2.

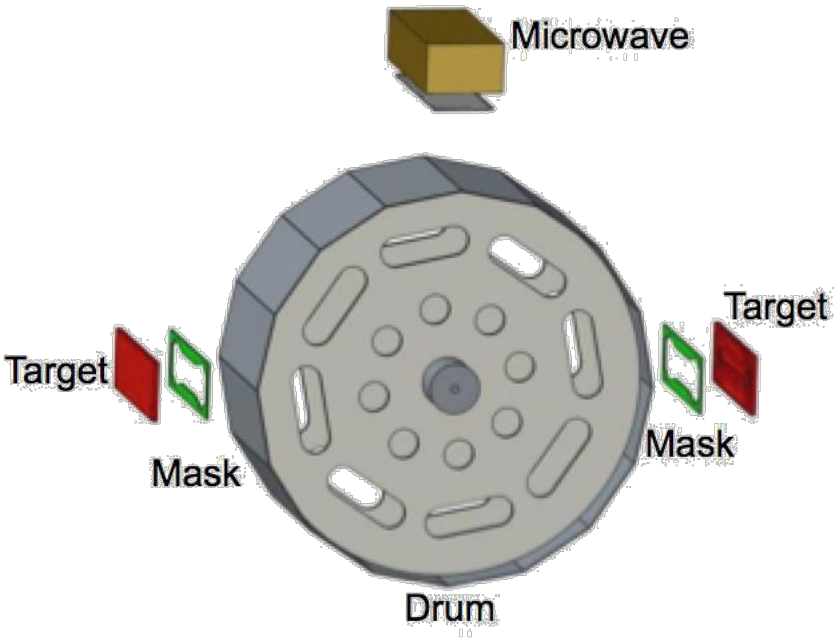
Microwave
Target
Target
Mask
Mask
Drum

3.

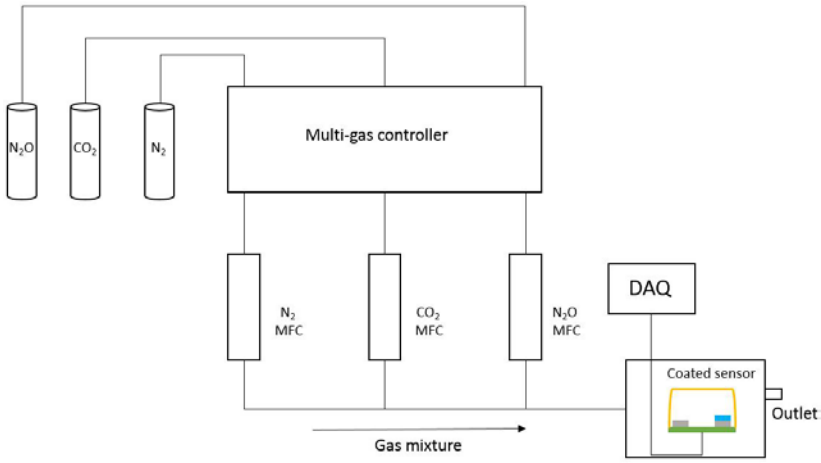
N_2O
CO_2
N_2
Multi-gas controller
N_2 MFC
CO_2 MFC
N_2O MFC
DAQ
Coated sensor
Outlet
Gas mixture

4.

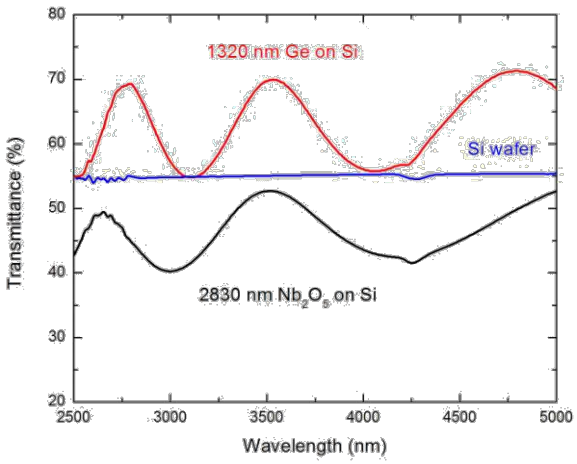
1320 nm Ge on Si
Si wafer
2830 nm Nb_2O_5 on Si
Transmittance (%)
Wavelength (nm)

5.

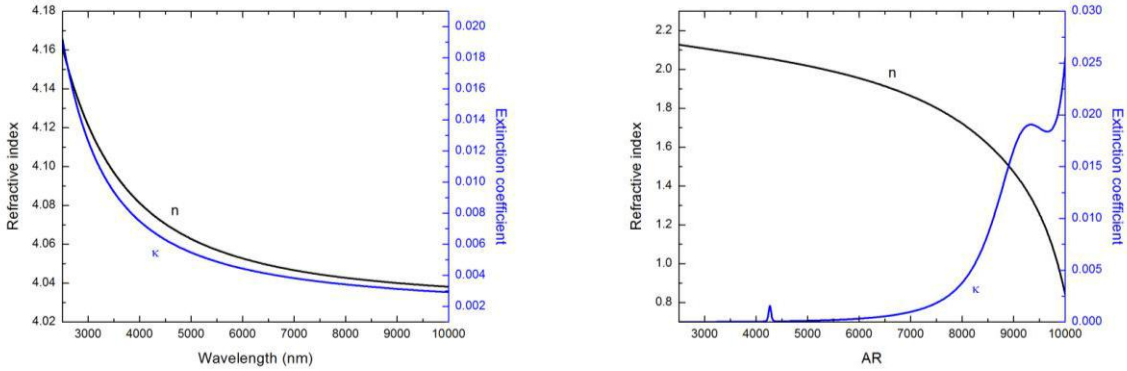
Refractive index
Extinction coefficient
Wavelength (nm)
n
κ
AR

(a) (b)

6.

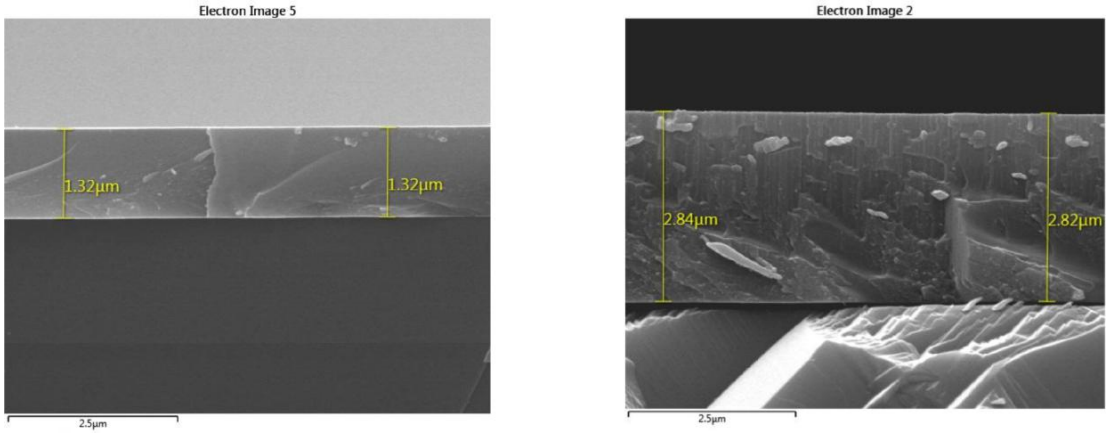
Electron Image 5
1.32µm
1.32µm
Electron Image 2
2.84µm
2.82µm

(a) (b)

7.

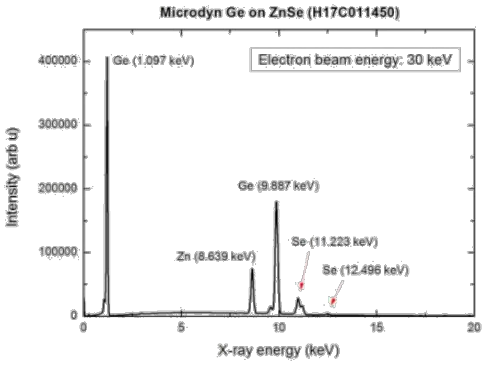
Microdyn Ge on ZnSe (H17C011450)
Electron beam energy: 30 keV
Ge (1.097 keV)
Ge (9.887 keV)
Zn (8.639 keV)
Se (11.223 keV)
Se (12.496 keV)
Intensity (arb u)
X-ray energy (keV)

(a)

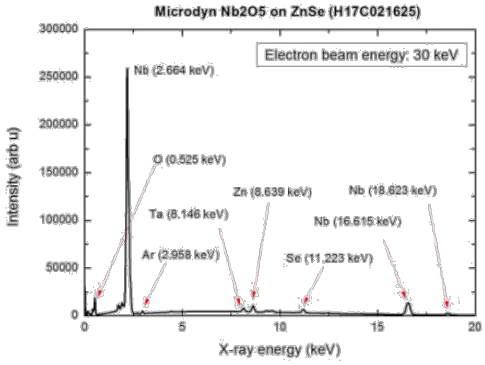
Microdyn Nb2O5 on ZnSe (H17C021625)
Electron beam energy: 30 keV
Nb (2.664 keV)
O (0.525 keV)
Ta (8.146 keV)
Ar (2.958 keV)
Zn (8.639 keV)
Se (11.223 keV)
Nb (16.615 keV)
Nb (18.623 keV)
Intensity (arb u)
X-ray energy (keV)

(b)

8.

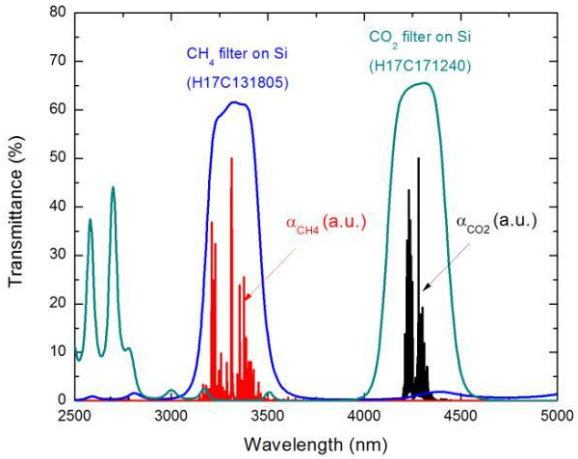
CH4 filter on Si
(H17C131805)
CO2 filter on Si
(H17C171240)
αCH4 (a.u.)
αCO2 (a.u.)
Transmittance (%)
Wavelength (nm)

9.

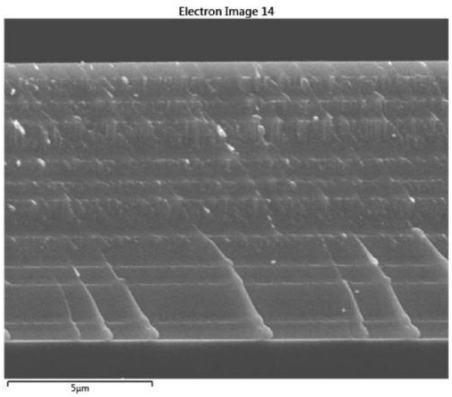
Electron Image 14
5μm

(a)

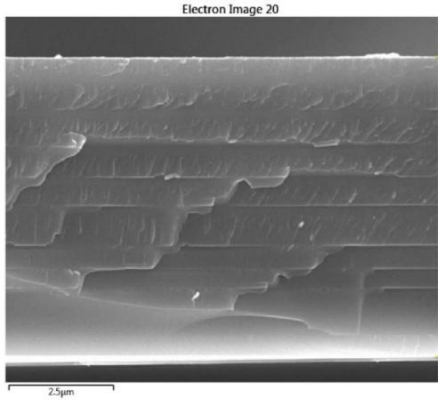
Electron Image 20
2.5μm

(b)

10.

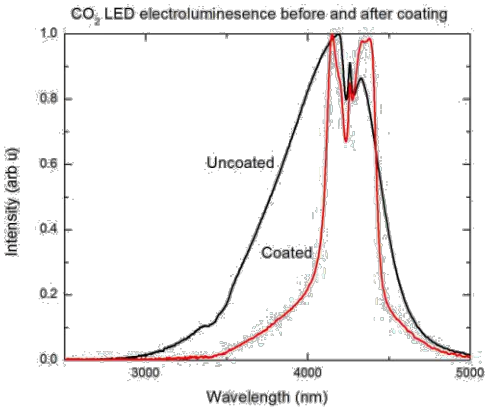
CO2 LED electroluminesence before and after coating
Intensity (arb u)
Wavelength (nm)
Uncoated
Coated

(a)

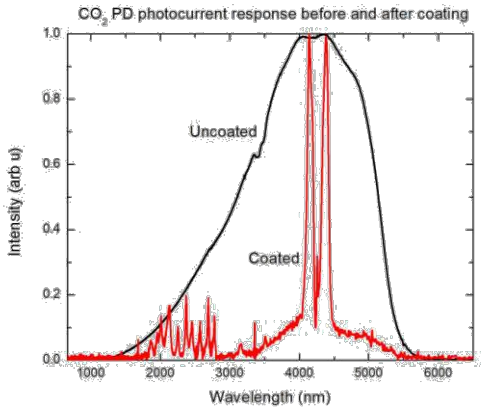
CO2 PD photocurrent response before and after coating
Intensity (arb u)
Wavelength (nm)
Uncoated
Coated

(b)

11.

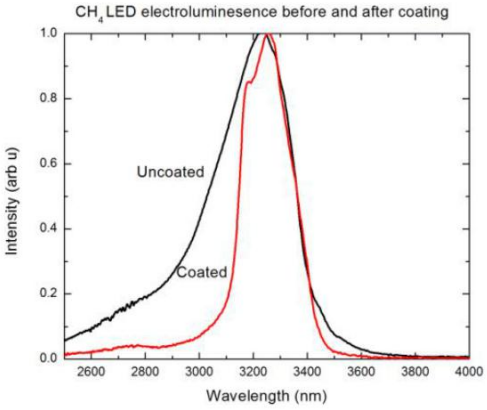
CH4 LED electroluminesence before and after coating
Intensity (arb u)
Wavelength (nm)
Uncoated
Coated

(a)

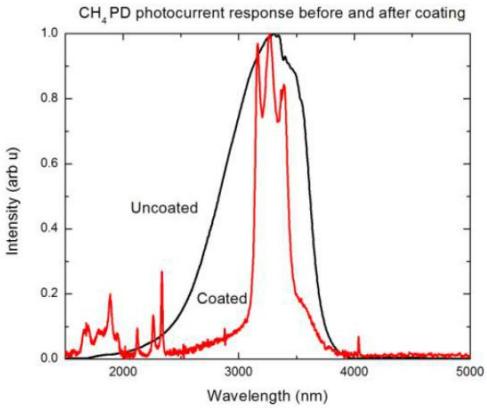
CH4 PD photocurrent response before and after coating
Intensity (arb u)
Wavelength (nm)
Uncoated
Coated

(b)

12.

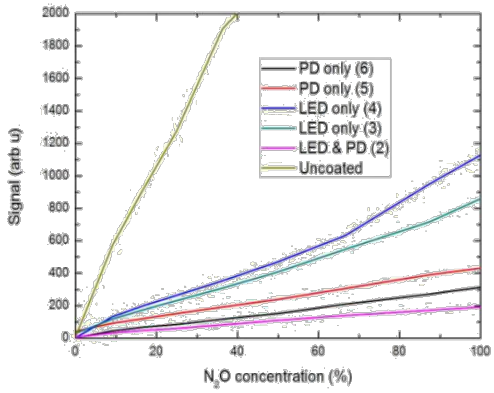
Signal (arb u)
N2O concentration (%)
PD only (6)
PD only (5)
LED only (4)
LED only (3)
LED & PD (2)
Uncoated

(a)

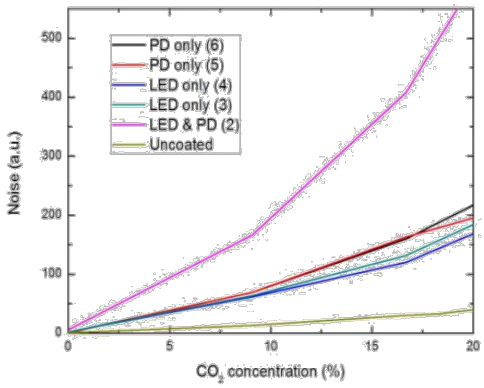
Noise (a.u.)
CO2 concentration (%)
PD only (6)
PD only (5)
LED only (4)
LED only (3)
LED & PD (2)
Uncoated

(b)

13.

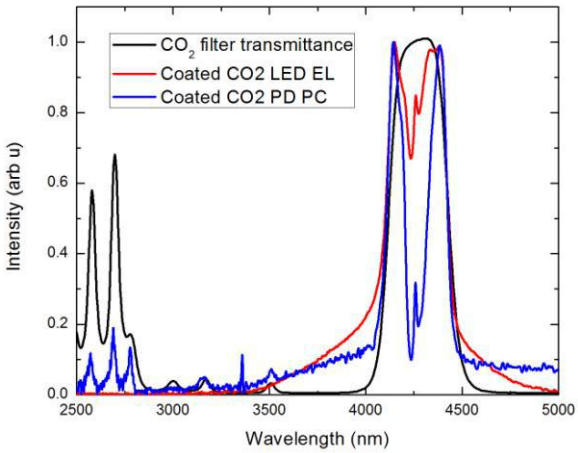
Intensity (arb u)
Wavelength (nm)
CO2 filter transmittance
Coated CO2 LED EL
Coated CO2 PD PC

14.

***Suggested Reviewers**

Marcela Bilek	The University of Sydney	marcela.bilek@sydney.edu.au
Zoe Barber	Reactive Sputtering Consulting	marcela.bilek@sydney.edu.au
Joerg Patscheider	EMPA	marcela.bilek@sydney.edu.au